

Current distribution and chirality in the regime of the quantized Hall effect

Serkan Sirt,¹ Matthias Kamm,¹ Vladimir Y. Umansky,² and Stefan Ludwig^{1,*}

¹Paul-Drude-Institut für Festkörperelektronik, Leibniz-Institut im Forschungsverbund Berlin e.V., Hausvogteiplatz 5-7, 10117 Berlin, Germany

²Weizmann Institute of Science, Rehovot 76100, Israel

The integer quantum Hall effect (QHE) is one of the most basic and, at the same time, astonishing phenomena in condensed matter physics. Despite its importance for metrology and fundamental physics, our microscopic understanding of the QHE is not yet complete. For decades, there has been a discussion about the current distribution inside a Hall bar for the case of a quantized Hall resistance. With the advent of quantum technology, the questions, if the current flows in compressible Landauer-Büttiker edge channels or in incompressible strips with varying geometry and whether the current flow is chiral or not, gain importance, because the quantum phase of each charge carrier depends on its exact pathway. In the present work, we compare multi-terminal current measurements in the regime of the QHE with model calculations in order to unravel the current density distribution in a Hall-bar device. We find, that the conjecture of chirality is justified for the plateaus of quantized Hall resistance, while in between plateaus the current density loses its chirality. The latter is described by the Drude model, which predicts a homogeneous current density for a sample with homogeneous mobility and carrier density.

I. INTRODUCTION

Magnetic field is an axial vector and, therefore, breaks time-reversal symmetry, which, however, can be restored by the simultaneous reversal of magnetic field and time, $\vec{B} \rightarrow -\vec{B}$ and $t \rightarrow -t$. This property gives rise to the chiral trajectory of a free charged particle in a homogeneous magnetic field, the mirror symmetry of the current in a two-terminal measurement, $I(\vec{B}) = I(-\vec{B})$, or the point symmetry of the Hall voltage, $V_H(\vec{B}) = -V_H(-\vec{B})$. The axial character of \vec{B} is expressed in terms of the vector product of the Lorentz force $\vec{F}_L = -e\vec{v} \times \vec{B}$ in the classical equation of motion $m\vec{\ddot{v}} = -e\vec{E} + \vec{F}_L$ of an electron with charge $-e$ and effective mass m at the momentary velocity \vec{v} , exposed to the fields \vec{E} and \vec{B} . As an introduction, we discuss the dynamics of charge carriers considering a variety of boundary conditions.

The solution for a *ballistic electron* is an in-plane spiral-shaped trajectory composed of a constant drift velocity $\vec{v}_d = \vec{E} \times \vec{B}/B^2 \neq \vec{v}$ and a cyclotron motion with radius $R_c = |\vec{v}|/\omega_c$, where $\omega_c = eB/m$ is the cyclotron frequency, cf. Fig. 1(a). The chirality of this trajectory is left-handed for the negatively charged electron (but would be right handed for a positive charge). Note that we define the chirality of a trajectory in analogy to the handedness of a screw thread.

The Drude model describes magnetotransport in the classical limit of the *diffusive regime*. Its key parameter is the electron mobility μ . For $\mu B < 1$ (corresponding to a mean-free path $l_m < R_c$), the cyclotron motion is impeded by Markovian momentum scattering. Consequently, the Drude model neglects the cyclotron motion by assuming $\vec{v} = \vec{v}_d$ and applying the relaxation ansatz $\vec{\ddot{v}}_d = \vec{v}_d/\tau$, where $\tau = m\mu/e$ is the momentum scattering time. In this diffusive limit and for $\vec{B} \perp \vec{E}$, the solution of the equation of motion introduced above can be written as

$$\vec{v}_d = \frac{-\mu}{1 + (\mu B)^2} (\vec{E} - \vec{E} \times \mu \vec{B}). \quad (1)$$

[For $\vec{E} \not\perp \vec{B}$ there would be a third summand, namely $\mu^2(\vec{E} \cdot \vec{B})\vec{B}$, inside the parantheses.] Clearly, the current density $\vec{j} = -en_s\vec{v}_d$ is homogeneous as long as both the carrier density n_s and the mobility μ are homogeneous. However for finite B , \vec{j} is not parallel to \vec{E} , but bent by the Hall angle $\varphi = \angle(\vec{j}, \vec{E}) = \tan^{-1}(\mu B)$, cf. Fig. 1(b).

The ballistic limit discussed above is clearly beyond the scope of the Drude model. Indeed, for $\mu B \rightarrow \infty$, the friction forces in Eq. (1) become negligible compared to the Lorentz force and the drift velocity becomes independent of μ . Nevertheless for $\mu B \rightarrow \infty$, the drift velocity takes the value $\vec{v}_d \rightarrow \vec{E} \times \vec{B}/B^2$, which is identical to that of a ballistic electron. This observation encourages us to compare measurements with the Drude model even for $\mu B \gg 1$.

In the remainder of the article, we restrict ourselves to a two-dimensional electron system (2DES), which defines the xy -plane, and include boundaries of the 2DES and electron scattering. Furthermore, we consider an in-plane electric field $\vec{E} = (E_x, E_y, 0)$ and a perpendicular, homogeneous magnetic field $\vec{B} = (0, 0, B)$, corresponding to one of the most common set-ups for magnetotransport measurements. For simplicity, we restrict our general discussion to a homogeneous electron density and mobility inside the 2DES (away from the edges).

To discuss the *classical limit of the Hall effect*, we include two sample edges at $y = 0$ and $y = b$, such that the electrons are confined in the y -direction but move freely in the x -direction, cf. Fig. 1(c). In the steady state, we expect $j_y = 0$ everywhere even for $B \neq 0$, because the edges reflect electrons. Applying this condition to Eq. (1) we find $E_y = -\mu B E_x$ and $j_x = E_y/R_H$ with the Hall resistance defined as $R_H = -\frac{B}{n_s e}$.

The transversal field $E_y = \vec{\nabla} V_H$ is maintained by charge accumulation at the sample edges, which gives rise to the Hall voltage V_H . In the steady state, $-eE_y = -F_L$, i.e., the Lorentz force acting on a free electron is exactly canceled, and the electrons move as if no magnetic field was applied but only the longitudinal field E_x . For our homogeneous sample, the current density j_x is a constant and the current is $I = j_x b$, with b being the width of the Hall bar.

In a confined sample, the axial character of the magnetic

* ludwig@pdi-berlin.de

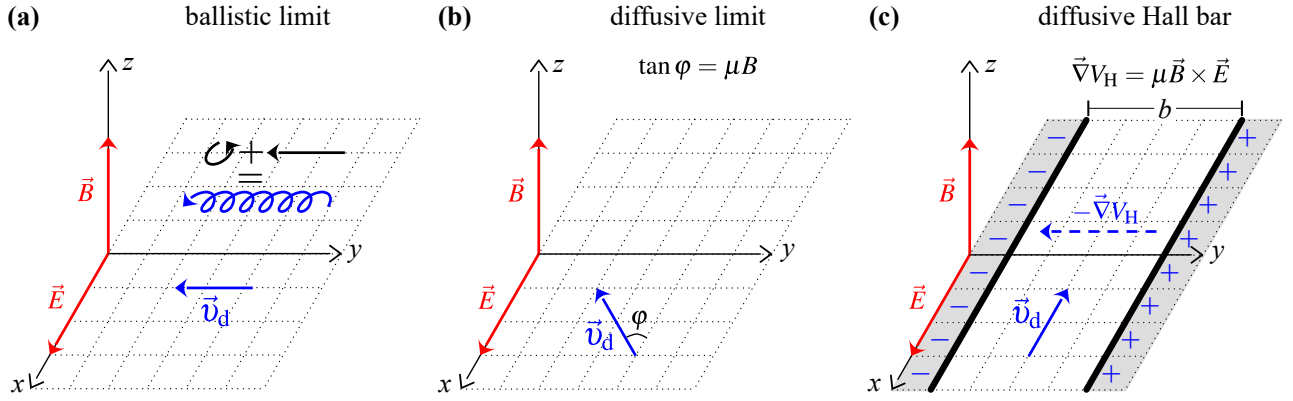


FIG. 1. Motion (expressed by drift velocity) of an electron confined to the xy-plane with in-plane electric and perpendicular magnetic fields, \vec{E} and \vec{B} (red arrows), respectively. (a) Ballistic limit (free electron). The spiral is the classical trajectory consisting of a constant drift velocity $\vec{v}_d = \vec{E} \times \vec{B} / B^2$ and a (left-handed) cyclotron motion with its radius being proportional to the initial velocity. (b) Diffusive limit. For $|\mu B| < 1$ the spiral motion is damped. However, the magnetic field reduces the drift velocity by the factor $1/\sqrt{1 + (\mu B)^2}$ and tilts it by the Hall angle ϕ . (c) Diffusive Hall bar in the steady state limit with edges parallel to the applied \vec{E} (red arrow). The Hall voltage compensates the Lorentz force, $-e\vec{\nabla} V_H = \vec{F}_L$ (or $E_y = |\vec{F}_L|/e$), such that the drift velocity is \vec{v}_d as for $\vec{B} = 0$.

field manifests itself in the edge charges or the related Hall voltage (which break the time reversal symmetry). The latter gives rise to an increase of the two-terminal resistance of the 2DES according to $R_{2T}(B) = \sqrt{R_0^2 + R_H^2}$ with the resistance R_0 of the 2DES at $B = 0$.

As we increase B , the quantization of the density of states into Landau-levels results in the *quantized Hall effect* (QHE). Its main features are plateaus of quantized Hall resistance accompanied by a vanishing longitudinal resistance. The latter indicates scattering-free transport within the Hall bar.

To explain the quantized values of R_H , the Landauer-Büttiker picture (LBP) assumes the formation of perfect one-dimensional (1D) edge channels, in which scattering is suppressed. The conductance of a spin-resolved 1D channel is e^2/h , which concurs with the observed quantization of the Hall resistance, $R_H = R_K/\nu$, in fractions of the von-Klitzing constant $R_K = h/e^2$. The filling factor ν describes the number of perfect 1D channels and is equal to two-times the filling fraction of the (spin-degenerate) Landau levels in the 2D bulk. The perfect 1D-channels are assumed to follow the edges of the Hall bar, because they form where the potential energy of the Landau levels, which increase towards the depleted sample edges, intersect with the Fermi level [1, 2]. To obtain a quantized Hall resistance, additionally the bulk (between the edge channels) is assumed to be insulating due to Anderson localization. The direction of the current flow in the edge channels is predetermined by the gradient of the confinement potential. This yields current flow in opposite directions at opposite edges. In that sense, in the LBP the QHE is associated with chiral current flow.

The LBP provides an intuitive explanation for the quantized Hall resistance and the vanishing longitudinal resistance of the QHE. While its merit is its simplicity, its predictions are limited due to the phenomenological character as well as its neglect of interactions and non-equilibrium effects. In particular,

the single particle assumption of the LBP leads to the prediction of a stepwise increase of the carrier density at the edges of the Hall bar because of the successive population of Landau levels [3, 4]. However, this would cause highly charged stripes between the edge channels corresponding to an unrealistically large Coulomb energy.

The screening theory [3–9] overcomes these limitations by taking into account the direct Coulomb interaction between the electrons. The Coulomb interaction causes a rearrangement of the free carriers such that the highly charged stripes are avoided. Instead, it leads to a segmentation of the Hall bar in compressible regions and incompressible strips (ICSs). Inside the ICSs, carriers cannot scatter and screening of the electric field is absent, because the chemical potential is in a local energy gap between filled and empty Landau levels; ICSs are accompanied by adjacent compressible regions, in which a Landau-level is aligned with the chemical potential, such that carriers can scatter. Inside the compressible regions, the electric field is then perfectly screened. The current flows where the electric field drops, i.e., inside the ICSs. In contrast to the 1D Landauer-Büttiker edge channels, the ICSs have a finite width exceeding the magnetic length [7–9]. Width and position of the ICSs depend on the magnetic field as well as the local electron density distribution $n_s(x, y)$ at $B = 0$. In particular, towards the end of each plateau with increasing magnetic field, the screening theory predicts a single extended incompressible region in the center of the Hall bar [7–9]. This implies that current can flow in the bulk of the Hall bar and not just in edge channels. The predicted bulk ICS near the high magnetic field end of the plateaus was experimentally corroborated in scanning gate spectroscopy experiments [10–12] and recently directly confirmed in transport experiments [13]. As we will discuss in Sec. IV below, the screening theory is consistent with chiral transport at the plateaus of the QHE, even if the current flows inside a single bulk ICS.

In the present article, we investigate the influence of a mag-

netic field on the current density distribution of a multiterminal junction. In Sec. II we illuminate the non-chiral character of the Drude model and derive a general coherent and chiral model. In Sec. III we compare our multi-terminal current measurements with the predictions of the models. For relatively small magnetic fields, we find that the classical limit of the Hall effect is described by the Drude model. For higher magnetic fields, we distinguish between the plateau regions of a quantized Hall resistance and the transition regions between plateaus. For the plateaus, coherent and chiral transport was already supported by Mach-Zehnder interferometer experiments measuring interference between two distinct current paths [14]. Our own results confirm this. For the magnetic field regions in between the plateaus our measurements are consistent with the predictions of the classical Drude model, which predicts non-chiral transport. In Sec. IV we explain, why the screening theory predicts chiral transport.

II. MODEL

In this section, we discuss the Drude model and, using the Landauer-Büttiker formalism (not to be confused with the LBP), derive a coherent and chiral model.

The magnetic field regions in between quantized plateaus deserve special attention. Because, near the plateaus of the QHE, the quantization of the density of states into Landau levels is relevant, we can classify these regions as belonging to the quantum regime. However, between plateaus, the electron transport is diffusive and our coherent and chiral model fails. In fact, the mobility $\mu(B)$ strongly oscillates, such that μB can be in the order of 1, as determined from the Shubnikov-de-Haas oscillations of the longitudinal resistance. Can we then apply the Drude model at large magnetic fields for the regions between quantized plateaus and is the magnetotransport between the plateaus chiral or not? In Sec. III we will provide an answer to these questions.

A. Drude model for a three-terminal junction

Using $\vec{j} = en_s \vec{v}_d$ we can rewrite Eq. (1) in terms of the magnetic-field-dependent conductivity tensor as

$$\begin{pmatrix} j_x \\ j_y \end{pmatrix} = \frac{\sigma_0}{1 + (\mu B)^2} \begin{pmatrix} 1 & -\mu B \\ \mu B & 1 \end{pmatrix} \begin{pmatrix} E_x \\ E_y \end{pmatrix}, \quad (2)$$

where the specific conductivity (defined at $B = 0$) is $\sigma_0 = en_s \mu$. For a laterally confined 2DES in the steady state, we assume $j_y = 0$, which implies $E_y = -\mu B E_x$ and, consequently, $j_x = \sigma_0 E_x = R_H^{-1} E_y$. Following the structure of the conductivity tensor, we divide the current density j_x into two components

$$j_x \equiv j_{xx} + j_{xy} \quad \text{with} \quad (3)$$

$$j_{xx} = \frac{en_s \mu}{1 + (\mu B)^2} E_x \quad \text{and} \quad j_{xy} = \frac{(\mu B)^2}{1 + (\mu B)^2} \frac{1}{R_H} E_y.$$

The longitudinal component $j_{xx} = \sigma_{xx} E_x$ is driven by the field E_x , which acts along the Hall bar because of its finite resistivity σ_0^{-1} . The transversal component $j_{xy} = \sigma_{xy} E_y$ is linked to the Hall voltage and attenuated by the Hall resistance. For $B = 0$ the component $j_{xy} = 0$, while for $\mu B \rightarrow \infty$ the current density becomes independent of μ as $j_{xx} \rightarrow 0$.

In experiments, we measure the current, which we find by integrating j_x across the Hall bar, $I = \int_0^b j_x dy$ ($= b j_x$ for a homogeneous Hall bar). Analogous to Eq. (3), we can write

$$I = I_{xx} + I_{xy} \quad \text{with} \quad (4)$$

$$\frac{I_{xx}}{I} = \frac{1}{1 + (\mu B)^2} \quad \text{and} \quad \frac{I_{xy}}{I} = \frac{(\mu B)^2}{1 + (\mu B)^2}.$$

Using $V_x = \int_{\text{Hall bar}} E_x dx$ and $V_H = \int_0^b E_y dy$, we find in addition $I = V_x/R_0 = V_H/R_H$, where we introduced the Hall bar resistance at zero magnetic field R_0 . I_{xx} corresponds to j_{xx} and I_{xy} corresponds to j_{xy} . We find $I = I_{xx}$ for $B = 0$, while $I \rightarrow I_{xy}$ for $B \rightarrow \infty$.

First, we discuss the current components I_{xx} and I_{xy} for the relatively simple case of a symmetric three-terminal junction as sketched in Fig. 2. We apply a voltage V_1 to contact 1 while the other two contacts are connected to the electrical ground, $V_2 = V_3 = 0$. Each contact has an ohmic contact resistance $R_{1,2,3}$ and we apply a finite magnetic field perpendicular to the conducting plane and pointing into it. We can measure the currents $I_{1,2,3} = I_{xx}^{(1,2,3)} + I_{xy}^{(1,2,3)}$. They fulfill Kirchhoff's junction rule $I_1 + I_2 + I_3 = 0$ also for the components $I_{xx}^{(1)} + I_{xx}^{(2)} + I_{xx}^{(3)} = 0$, $I_{xy}^{(1)} + I_{xy}^{(2)} + I_{xy}^{(3)} = 0$, because the respective driving fields are perpendicular to each other. The longitudinal component $-I_{xx}^{(1)}$ will be divided between contacts 2 and 3 according to Ohm's law as indicated in Fig. 2(a): $I_{xx}^{(2,3)} = -I_{xx}^{(1)} \frac{R_{3,2}}{R_2 + R_3}$. The transversal component $-I_{xy}^{(1)}$ follows the charged edge of the Hall bar and is accordingly bent into contact 2 (or into contact 3 for \vec{B} pointing out of the plane). In Fig. 2(b), we indicate the transversal component for the simplified case of a vanishing contact resistance, $R_2 = 0$, resulting in $I_{xy}^{(2)} = -I_{xy}^{(1)}$ and $I_{xy}^{(3)} = 0$.

In a realistic device with finite contact resistances, the voltage drop across each contact resistance causes a partial reflection at each contact. Therefore, a smaller fraction of $-I_{xy}^{(1)}$ flows from contact 2 to contact 3 as shown in Fig. 2(c). Because the magnitude of $I_{xy}^{(1)}$ is predetermined by the applied voltage and the Hall resistance, we can express the division of $-I_{xy}^{(1)}$ in terms of two parallel channels with the effective resistances R_2 versus $R_H + R_3$. Hence, we have $I_{xy}^{(2)} = -I_{xy}^{(1)} \frac{R_H + R_3}{R_H + R_2 + R_3}$ and $I_{xy}^{(3)} = -I_{xy}^{(1)} \frac{R_2}{R_H + R_2 + R_3}$.

The ohmic components $I_{xx}^{(1,2,3)}$ vanish quickly for $\mu B \gg 1$. The transversal currents $I_{xy}^{(1,2,3)}$ vanish at $B = 0$, but for $\mu B \gg 1$ the current density distribution merits a closer look. On the one hand, away from a junction, the Drude model predicts a homogeneous current density across a homogeneous sample, cf. Eq. (1), classifying j_x to be non-chiral. On the other hand, near a junction, the edge charges caused by the Lorentz force break the homogeneity of the transversal current density j_{xy} , while the current I_{xy} is bent into just one of the branches of

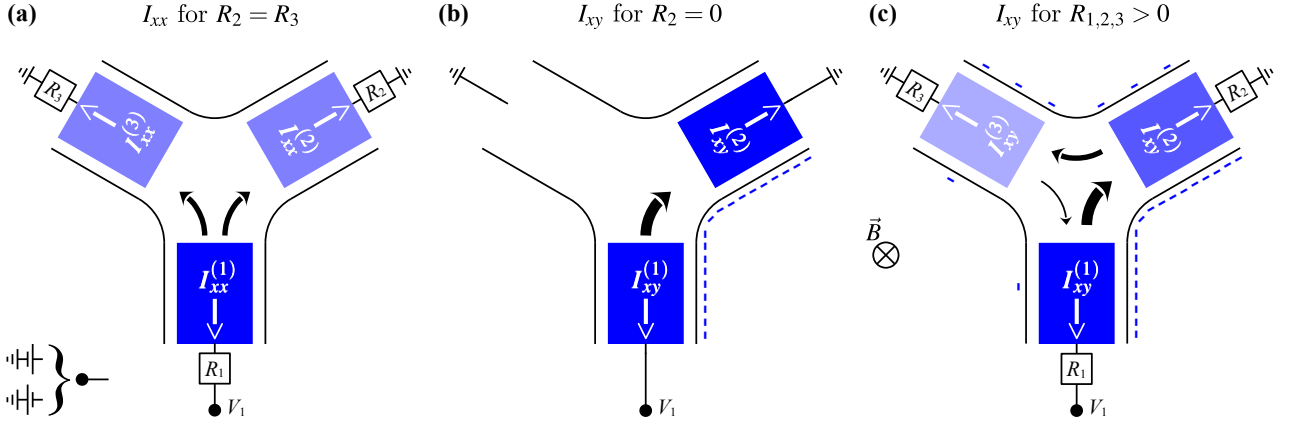


FIG. 2. Drude model: Distribution of current $I = I_{xx} + I_{xy}$ in a three-terminal device with homogeneous electron density and mobility in the diffusive and classical limit for $V_1 \neq 0$, $V_2 = V_3 = 0$, $R_2 = R_3$ and \vec{B} pointing into the plane of the 2DES. Color intensities indicate the distribution of the absolute value of the current density into the three branches. Within each branch, the current density is homogeneous. For $V_1 < 0$, white arrows show the directions of the conventional currents and black bent arrows the direction and relative magnitudes of electron flow (for $V_1 > 0$ vice versa). (a) I_{xx} displaying ohmic behavior, the same as for $B = 0$: $I_{xx}^{(2)} = I_{xx}^{(3)} = -0.5I_{xx}^{(1)}$. (b) I_{xy} for $R_2 = R_3 = 0$ displaying non-ohmic behavior: $I_{xy}^{(2)} = -I_{xy}^{(1)}$ and $I_{xy}^{(3)} = 0$. (c) I_{xy} for $R_2 = R_3 > 0$: I_{xy} is still bent by the Lorentz force but partly reflected at the resistive contacts: $I_{xy}^{(2)} > I_{xy}^{(3)}$ with $I_{xx}^{(2)} + I_{xx}^{(3)} = -I_{xx}^{(1)}$. The distribution of I_{xy} resembles chiral behavior but I_{xy} is homogeneous in each branch (away from the junction region).

the junction. Finally, if considering the currents flowing out of each contact in a measurement at $\mu B \gg 1$, practically being a measurement of the transversal components $I_{xy}^{(1,2,3)}$, we expect to find identical result whether the transport is chiral or not. Hence, an experimental indication of non-chiral transport in a multiterminal current measurement can only be expected for $\mu B \lesssim 1$, where the homogeneous j_{xx} is sizable.

B. Coherent and chiral model of n -terminal device

Next, we derive a general model for the current in a 2DES device prepared in the coherent and chiral limit but equipped with n ohmic contacts, cf. Fig. 3. The model intends to describe current flow through a Hall bar in the region of a quantized plateau. The inner circle in Fig. 3 indicates the coherent 2D conductor, the radial lines symbolize the n terminals $i = 1, 2, \dots, n$. External voltages V_i can be applied to the contacts in respect to ground, while $V'_i = V_i + I_i R_i$ are the voltages present at the intersects of the coherent part of the sample and each contact. The current I_i flows through the i th contact with ohmic resistance R_i to ground.

To describe the coherent inner part of the sample, we employ the Landauer-Büttiker formalism and write

$$I_i = \sum_{j=1}^n G_{ij} V'_j = (V'_i - V_i)/R_i, \quad (5)$$

where G_{ij} are the coherent conductance coefficients, which can be formally derived from the scattering matrix of the problem. Assuming chiral transport, current flows only between adjacent contacts. The direction of the chirality is linked to the direction of the magnetic field vector. In our case as sketched

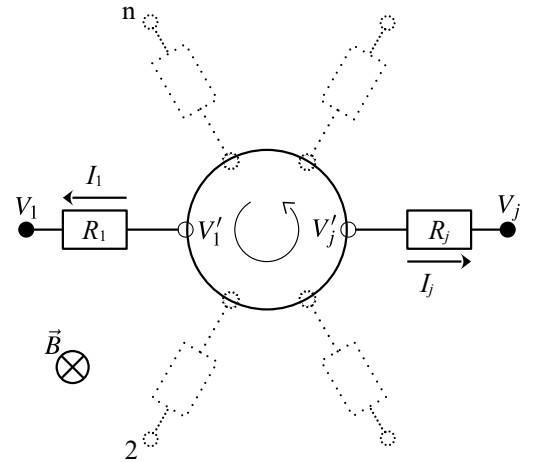


FIG. 3. Simplified circuit diagram of an n -terminal device. The inner circle indicates coherent and chiral current flow inside the 2DES. Each contact $i = 1, \dots, n$ has an ohmic resistance R_i and a voltage V_i applied in respect to the electrical ground. V'_i are the voltages resulting at the intersections of the ohmic contacts and the coherent inner circle. The magnetic field vector pointing into the plane of the 2DES gives rise to a right handed chirality of a free charge which translates into a left handed chirality of the device, cf. circled arrow.

in Fig. 3, we consider \vec{B} pointing into the plane of the 2DES, such that $G_{ij} = 1$ and $G_{ji} = 0$ for $i = j + 1$. The unitarity of the scattering matrix implies $\sum_i G_{ij} = \sum_j G_{ij} = 0$, such that

our chiral conductivity tensor takes the form

$$G_{ij} = \nu G_0 \begin{cases} 1; & i = j + 1 \\ -1; & i = j \\ 0; & \text{else} \end{cases}, \quad (6)$$

where $G_0 = e^2/h$ and ν is the filling factor of the (spin-resolved) Landau-levels. The coherent limit applies for the quantized plateaus of the Hall resistance, where ν is an integer. Inserting Eq. (6) into Eq. (5) and solving the equation system yields the currents

$$I_i = \frac{V'_i - V_i}{R_i} \quad \text{with} \quad V'_i = \frac{1}{P_i} \left(\frac{S_n}{P_n - 1} + S_i \right) \quad (7)$$

where we introduced

$$P_i = \begin{cases} \prod_{j=1}^i \left(1 + \frac{1}{\nu G_0 R_j} \right); & i = 1, 2, \dots, n \\ 1; & i = 0 \end{cases}$$

and

$$S_i = \sum_{j=1}^i P_{j-1} \frac{V_j}{\nu G_0 R_j}.$$

Equation (7) describes the current distribution into the n ohmic contacts of a chiral and coherent sample. For $V_1 \neq 0$ but all other applied voltages $V_{i>1} = 0$ the currents can be written as

$$I_{i>1} = \frac{P_n/P_i}{1 - P_n/P_1} \frac{1}{\nu G_0 R_i} I_1,$$

which are independent of R_1 as expected.

C. Drude model of n -terminal device

Our model describing coherent currents is based on the unitarity of the scattering matrix. However, regarding the actual macroscopic currents into various contacts, the unitarity condition implies the same result as we find from applying Kirchhoff's laws. Therefore, if we replace R_H by $(\nu G_0)^{-1}$, for $n = 3$ and $V_2 = V_3 = 0$, Eq. (7) of the coherent and chiral model predicts the identical currents $I_{2,3}$ as the transversal current component $I_{xy}^{(2,3)}$ of the Drude model discussed in Sec. II A above. By extrapolating this observation, we can expand our prediction of the Drude model for the current distribution of an n -terminal junction and find

$$\begin{aligned} I_i &= \frac{1}{1 + (\mu B)^2} I_{xx}^{(i)} + \frac{(\mu B)^2}{1 + (\mu B)^2} I_{xy}^{(i)} \quad \text{with} \\ I_{xx}^{(i)} &= \frac{1}{R_i} \left[\frac{\sum_{m=1}^n V_m / R_m}{\sum_{m=1}^n 1 / R_m} - V_i \right] \\ I_{xy}^{(i)} &= \frac{1}{R_i} \left[\frac{1}{P_i} \left(\frac{S_n}{P_n - 1} + S_i \right) - V_i \right]. \end{aligned} \quad (8)$$

The longitudinal component, $I_{xx}^{(i)}$, is determined by Ohm's law while the transversal component, $I_{xy}^{(i)}$, is identical to Eq. (7), where we use $R_H = (\nu G_0)^{-1}$.

To correctly describe the regions of the plateaus of a quantized Hall resistance, we use constant and integer ν and assume $\mu = \infty$, a property of ballistic transport, such that $I_{xx}^{(i)} = 0$. Then Eq. (8) is identical to Eq. (7).

III. EXPERIMENTAL RESULTS AND DISCUSSION

Multiterminal current measurements yield the distribution of the current into the different contacts. In this section, we compare the results of multi-terminal measurements and theory predictions in a wide magnetic field region corresponding to $1 \lesssim \nu < \infty$. We will see, that multiterminal measurements can provide answers to the questions about chirality and the local current distribution in magnetotransport.

A. Sample and measurement setup

We use a Hall bar as sketched in Fig. 4. It is etched

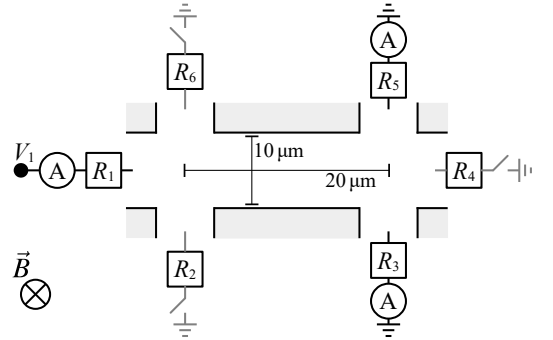


FIG. 4. Sketch of a Hall bar with six contacts, characterized by their ohmic resistances, R_i . We apply a voltage V_1 to contact 1 and measure currents into contacts 1, 3, and 5. Contacts 2, 4, and 6 can be left floating or connected to electrical ground. Current amplifiers at contacts 3 and 5 result in additional voltages of $\simeq 20 \mu\text{V}$ applied to contacts 3 and 5 (not shown, but taken into account for generating model curves). \vec{B} points into the plane of the 2DES.

from a GaAs/(Al,Ga)As heterostructure, which contains a two-dimensional electron system (2DES) 130 nm beneath the surface. We performed the experiments at a temperature of $T \simeq 300 \text{ mK}$ in a He-3 evaporation cryostat. At this temperature and zero magnetic field, the electron density and mobility of the 2DES, determined from Hall measurements, are $n_s \simeq 1.2 \times 10^{11} \text{ cm}^{-2}$ and $\mu \simeq 3.95 \times 10^6 \text{ cm}^2/\text{Vs}$ (yielding a mean-free-path of $\lambda_m \simeq 23 \mu\text{m}$), respectively.

For multi-terminal current measurements, we apply the voltage of $V_1 = \pm 1 \text{ mV}$ to the source contact 1 (using a Keithley 2450 source meter). We measure the current $I_1(B)$ flowing from the Hall bar into contact 1, using the source meter, and the currents $I_3(B)$ and $I_5(B)$ flowing into contacts 3

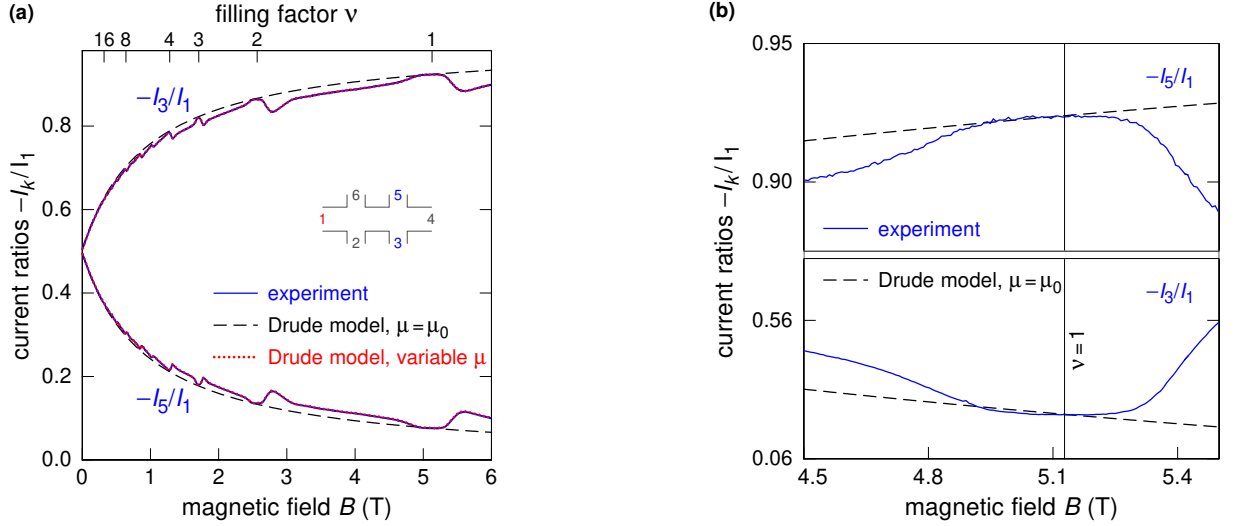


FIG. 5. Three-terminal measurement with symmetric circuit, cf. inset in (a). A voltage of $V = 1$ mV is applied to contact 1, while contacts 3 and 5 are connected to ground via current amplifiers; contacts 2, 4, and 6 are electrically floating. \vec{B} points from the surface into the 2DES plane such that I_{xy} is bent towards contacts 2 and 3. (a) Current ratios $-I_3/I_1$ and $-I_5/I_1$ as a function of magnetic field B (solid blue lines); Drude model prediction of Eq. (8) assuming constant $\mu = \mu_0$ (dashed black line); fit of Drude model prediction of Eq. (8) with $\mu(B)$ as free parameter (dotted red line). (b) enlargements near $\nu = 1$ showing experimental data and the Drude model prediction for $\mu = \mu_0$.

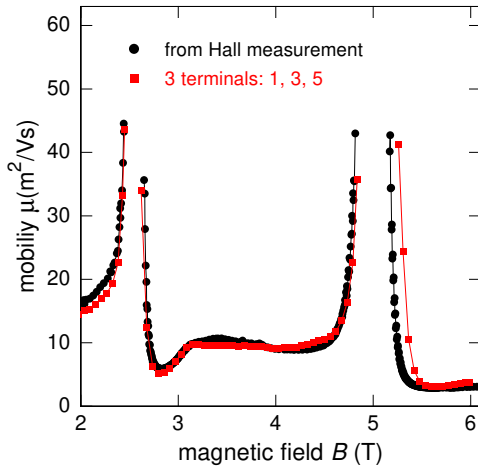


FIG. 6. Mobility $\mu(B)$ as determined from SdH-oscillations of the longitudinal resistance between contacts 2 and 3 (black dots) in comparison with $\mu(B)$ found by fitting Eq. (8) to the three-terminal measurements shown in Fig. 5 (red squares).

or 5, respectively, using Basel Precision Instr. current amplifiers. Contacts 3 and 5 are connected to the electrical ground, while the remaining contacts 2, 4, and 6 may be either electrically floating or connected to ground depending on the experiment, cf. Fig. 4. Here, we apply B perpendicular to the 2DES, such that it points from the sample surface towards the 2DES, hence, electrons contributing to I_{xy} move from contact to contact along the counterclockwise pathway $1 \rightarrow 2 \rightarrow 3 \rightarrow 4 \rightarrow 5 \rightarrow 6 \rightarrow 1$. Due to the direction of the magnetic field and a voltage applied to contact 1, the largest

portion of I_{xy} will always flow between contact 1 and contact 3, if contact 2 is floating, or to contact 2, if it is grounded. Whether this current is positive or negative depends on the sign of V_1 .

We performed a series of measurements at $B = 0$ to determine the contact resistances ($R_i \sim 2.5$ k Ω) and offset voltages ($V_{3,5} \sim 20$ μ V) of the two current amplifiers. In addition, we used the comparison between measured data and model curves for a fine tuning of these circuit parameters, which remain constant between measurements. They are listed in Table I.

| contact i | resistance R_i (Ω) | voltage V_i (mV) | geometry a_i |
|-------------|-------------------------------|--------------------|----------------|
| 1 | 2420 | 1.000 | 1 |
| 2 | 2420 | 0 | 0.5 |
| 3 | 2400 | -0.021 | 1 |
| 4 | 2350 | 0 | 1 |
| 5 | 2420 | -0.018 | 1 |
| 6 | 2400 | 0 | 0.5 |

TABLE I. Parameters of the circuit sketched in Fig. 4. Contact resistances R_i include ohmic contacts, cables and RC-filters. Voltage V_1 is applied to contact 1, V_2 and V_3 are offset voltages of the current amplifiers. To account for the contribution of the Hall bar itself to the resistance, we defined a geometry parameter and use $R_i \rightarrow R_i + a_i/[n_s e \mu(B)]$ in the model calculations of the ohmic contributions. The correction is negligible for $B = 0$.

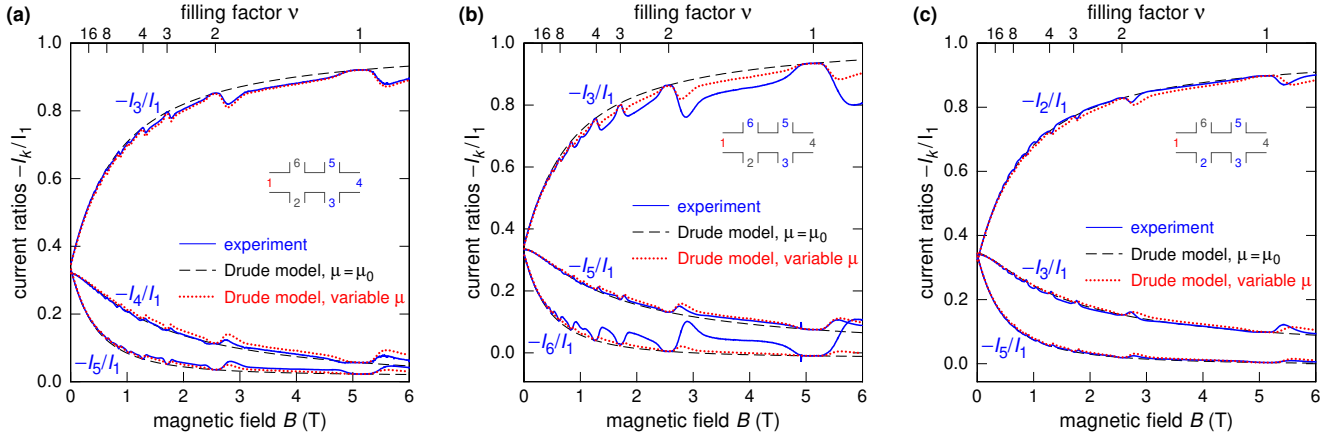


FIG. 7. Four-terminal measurements for three different contact configurations, cf. insets, further configurations and labeling as in Fig. 5. (a) symmetric four-terminal circuit. (b) and (c) variations of asymmetric four-terminal circuits.

B. Three-terminal measurements

First, we discuss a three-terminal measurement in a mirror symmetric geometry, for which we keep the contacts 2, 4 and 6 electrically floating; current flows from contact 1 into contacts 3 and 5. In Fig. 5(a), we present as solid (blue) lines the measured current ratios $-I_3(B)/I_1(B)$ and $-I_5(B)/I_1(B)$. As expected, we find that $|I_3|$ increases with B while $|I_5|$ decreases accordingly, such that $I_3(B) + I_5(B) = -I_1(B)$. The dashed black line indicates the prediction of the Drude model according to Eq. (8) for $n = 3$ if we assume a constant mobility $\mu(B) = \mu_0 \equiv \mu(B = 0) = 395 \text{ m}^2/\text{Vs}$. For this large mobility, the Ohmic term (first term) of Eq. (8) can be neglected for $B \gtrsim 50 \text{ mT}$ (corresponding to $\mu B \gtrsim 20$). In this limit, with $(\nu G_0)^{-1} = R_H(B)$, Eq. (8) becomes identical to the coherent chiral model expressed in Eq. (7).

The Drude model and the measured data agree in the classical limit for $B \lesssim 0.5 \text{ T}$. As we increase B further, the Drude model with a constant $\mu(B) = \mu_0$ still predicts the correct trend, but we observe growing deviations for filling factors away from integer values [top axis of Fig. 5(a)]. The enlargement around the first plateau of the QHE in Fig. 5(b) clarifies, that model and experiment match exactly only at specific values of B including integer bulk filling factors (here $\nu = 1$). An exact match between measurements and model can be achieved by using $\mu(B)$ as a free fit parameter in Eq. (8). For the dotted red line in Fig. 5(a), we used the magnetic field dependent values of $\mu(B)$ as shown by red squares in Fig. 6. For comparison, we have also determined $\mu(B)$ from the Shubnikov-de-Hass oscillations of a standard longitudinal resistance measurement, see the black dots in Fig. 6. [15] The agreement between the $\mu(B)$ values obtained from longitudinal resistance measurements with those obtained by fitting Eq. (8) to our three-terminal current measurements supports the validity of our model.

The two regions of divergent $\mu(B)$ in Fig. 6 correspond to the plateau regions at $\nu = 2$ and $\nu = 1$. Here, $I_{xx} = 0$ and the coherent and chiral model expressed in Eq. (7) is valid. Away

from the plateau regions, we find strongly reduced mobility values with $1 \lesssim \mu < 20$, which indicate diffusive transport and a finite ohmic contribution I_{xx} to the current.

The overall agreement between the prediction of Eq. (8) and our three-terminal measurements is convincing. On the one hand, it supports the assumption of coherent and chiral transport for the quantized plateaus of the Hall resistance. On the other hand, it points to non-chiral transport described by the Drude model not only in the classical regime of the Hall effect but also for large B in between the plateaus.

C. Four-terminal measurements

In Fig. 7, we present current ratios $-I_i/I_1$ for three different four-terminal measurements. Again, we measure the currents into contacts $i = 1, 3$ and 5, but now we ground an additional contact, namely contact 4 in Fig. 7(a), contact 6 in (b), and contact 2 in (c). If we assume $\mu(B) = \mu_0$, Eq. (8) of the Drude model reproduces the overall dependences $I_i(B)$ with a similar accuracy as it did for the three-terminal measurement (dashed black lines). The dotted red lines correspond to the predictions of Eq. (8) using the identical $\mu(B)$ that we found by fitting the three-terminal measurement above, cf. Fig. 6. Again, for $B \lesssim 0.5 \text{ T}$, theory and experiment agree well. For $B > 0.5 \text{ T}$, the agreement is still perfect for the plateau regions but becomes worse away from the plateaus of quantized Hall resistance. experimental results is even worse (for $B > 0.5 \text{ T}$).

This observation allows two immediate conclusions: (1) for the plateau regions, the chiral transport already found in the three-terminal measurement is confirmed; (2) away from the plateaus, the non-chiral transport is also confirmed. However, for more than three terminals, the model prediction of Eq. (8) fails for $B > 0.5 \text{ T}$.

In Fig. 8, we plot for each of the three four-terminal measurements shown in Fig. 7 the branch corresponding to the largest current. We slightly scaled the data to compensate for small variations in the contact resistances. After scaling, the

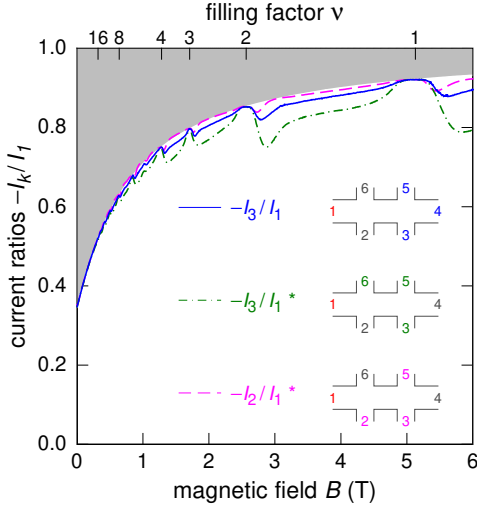


FIG. 8. Comparison of the respective largest measured current contributions flowing into a grounded contact for three different configurations of four-terminal measurements. The current ratios I_i/I_1 marked with a * are slightly scaled such that all three theory curves according to Eq. (8) with $\mu = \mu_0$ are identical following the edge between shaded and white backgrounds.

three curves are identical in the classical regime ($B < 0.5$ T) and on the plateaus of the QHE. The edge between shaded and white backgrounds corresponds to the prediction of the Drude model for constant $\mu = \mu_0$ [dashed black lines in Fig. 7(a)]. Compared to this model prediction, the current is reduced between the plateaus for all three geometries. The reduction is particularly strong for the set-up with contact 6 connected to ground. In the case of chiral transport, contact 6 is the last one to be reached by the current, while most current should flow into contact 3. The reduction of the current into contact 3 goes along with an enhancement of the current into contact 6, cf. Fig. 7(b). This is a clear signature of non-chiral current but, the current reduction into contact 3 (and the current enhancement into contact 6) exceeds even the prediction of our model expressed by Eq. (8). Likewise, for the set-up with contact 2 grounded, the reduction of the current into contact 2 is smaller than the reduction predicted by Eq. (8). So, a smaller amount of the non-chiral current reaches contact 5 as it is much further away from contact 1 than contact 2.

The details of the measured current distribution clearly depend on the contact configuration. This behavior demonstrates the limits of our model. For the derivation of Eq. (8), we assumed an infinitely long Hall bar without additional grounded contacts. Hence, for identical contact resistances, its prediction is independent of the variations between specific configurations of the four-terminal set-up (the resistance of the Hall bar itself at $B = 0$ is much smaller than the contact resistances). To overcome the failure of our simplified model, it would be necessary to account for the more complicated steady-state electrostatics of a multi-terminal device, in particular the inhomogeneity of the electric field near a junction. Suitable numerical calculations could clarify this

point. For the moment, we conjecture that such a corrected model would support our previous result based on the three-terminal measurement, namely that the Drude model correctly describes the transition regions between plateaus.

IV. SCREENING THEORY AND CHIRAL TRANSPORT

In this section, we restrict the discussion to the plateau regions of the quantized Hall resistance, for which our multiterminal experiments indicate chiral and coherent transport. The unique characteristics of chiral transport of a 2D conductor is the opposite directions of current flow along the opposite edges of the conductor. The QHE reveals the additional feature of fundamental resistance values being fractions of h/e^2 . These values can be measured with an extremely high accuracy and stability with deviations of less than 3×10^{-9} having been demonstrated between high resolution measurements of various samples in different laboratories [16]. In order to explain the measured highly accurate resistance values in fractions of h/e^2 , scattering has to be (almost) completely suppressed.

The LBP [1, 2] is a single-particle model based on the assumption that the Landau levels form perfect 1D edge channels, which support chiral transport, while the bulk of the 2DES is assumed to be electrically insulating because of disorder-induced localization. The edge channels are compressible, meaning that there exist occupied and unoccupied states at the chemical potential. The mere assumption of scattering free transport via compressible edge channels as an explanation of the extremely accurate measurements of the fundamental resistance value h/e^2 is unsatisfactory.

The screening theory offers an alternative explanation of the highly accurate resistance values in fractions of h/e^2 , which is based on first principle calculations [7–9]. Already the earliest purely classical considerations, taking into account the Coulomb interaction, led to the realization of a segmentation of the 2DES confined in a Hall bar in perfectly screened compressible regions and completely unscreened ICSs [3–6]. Inside the ICSs, scattering is forbidden because the excitation of a carrier costs the energy $\hbar\omega_c$ of the Landau gap. While numerous experiments already support the screening theory [10–13, 17–23], here our focus is on the question whether the screening theory is consistent with chiral transport.

In Fig. 9, we sketch the situation for the first plateau ($\nu = 1$, $I_{xx} = 0$) of the QHE for the case of a three-terminal junction. As a start, in Fig. 9(a), we show the situation assumed in the LBP. All current flows inside the compressible edge channels (solid blue lines). The stem towards contact 1 contains a sketch of the first Landau level (LL_1 , solid line), which strictly follows the confinement potential for the single particle LBP. The edge channels emerge, where LL_1 intersects with the chemical potential, which differs by V_H between the respective edges. The Hall potential $U_H = eV_H$ (dotted line) drops linearly between the edge channels.

To illustrate the screening theory [9], we consider the two limiting cases realized near the ends of the first plateau of the QHE. For simplicity, we neglect disorder effects. Near the

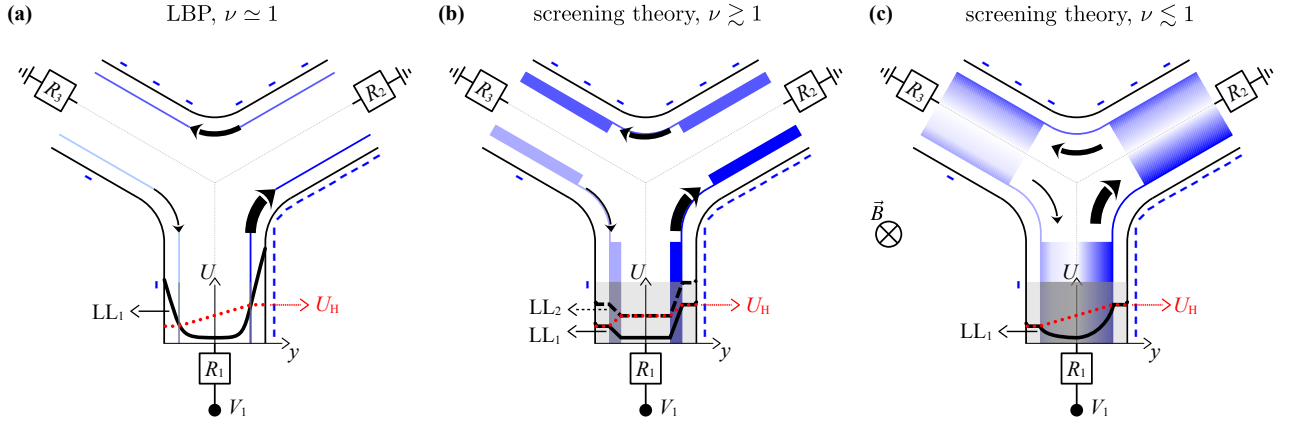


FIG. 9. Coherent and chiral models for the first plateau of the QHE: Sketch of the distribution of the current I_{xy} near $\nu = 1$ for $V_1 \neq 0$, $V_2 = V_3 = 0$, $R_2 = R_3$ with \vec{B} pointing into the plane of the 2DES. Color intensities indicate the distribution of the absolute value of the current density into the three branches. Black bent arrows show the direction and relative magnitudes of electron flow related with the charged edges indicated by blue minus signs for $V_1 < 0$. For $V_1 > 0$, current densities remain the same while the edge charges become positive and black arrows indicate the current flow. (a) Prediction of the Landauer Büttiker picture, assuming that current flows in one-dimensional chiral edge channels only. (b) Prediction of the screening theory for the case of edge ICSs (current flows inside ICSs only). (c) Prediction of the screening theory for the case of a bulk ICS. All three cases predict chiral current flow within the 2DES and result in identical currents I_1 , I_2 and I_3 into the contacts. In the stem towards contact 1 we sketch the electrochemical potentials of the first Landau level (LL_1 , solid line) and the related Hall potential (U_H , dotted red line).

lower magnetic field end with $\nu > 1$, the screening theory predicts two narrow ICSs roughly resembling Landauer-Büttiker edge channels, cf. Fig. 9(b). Near the high field end of the plateau, where $\nu \leq 1$, the prediction is a single bulk ICS, while the 2DES near the edges remains compressible, cf. Fig. 9(c). Even for the first case with two edge ICSs, in contrast to the LBP, the current flows entirely inside the ICSs, where scattering is suppressed due to the Landau gap of the density of states. In the compressible regions of the 2DES, electrons can scatter and the local electric field is perfectly screened. As a result, the local electric field entirely drops inside the ICSs. The gradient of the Landau levels, i.e., the effective local electric field drives the current according to $\vec{j} = -en_s \vec{E} \times \vec{B}/B^2$. Therefore, no current flows in the perfectly screened compressible regions. The gradient of the potential energy of the Landau levels equals the gradient of the local electric field. As can be seen in the sketches of the first Landau level in Figures 9b and 9c, the gradient of the Landau levels has opposite directions inside the ICS(s) along the opposite edges of the sample. This is even the case if only a single ICS covers most of the 2DES, cf. Fig. 9(c). Here, $\vec{E} = 0$ and $\vec{j} = 0$ in the center of the ICS and the current flows in opposite directions on both sides of the ICS. Consequently, even in case of a single bulk ICS, the current flow is still chiral and the local current density is larger near the sample edges, where the confinement potential drops steeply.

V. SUMMARY AND OUTLOOK

In summary, we have performed multi-terminal current measurements in the regime of the QHE and compared our

results with predictions of a coherent and chiral model versus the Drude model. The Drude model perfectly describes our results in the classical regime of small magnetic fields, the coherent and chiral model fits for the regions corresponding to quantized plateaus of the Hall resistance. In the diffusive regions for large magnetic fields, i.e., between quantized plateaus our three-terminal experiment supports the predictions of the Drude model, which includes non-chiral transport. The four-terminal measurements demonstrate the limits of our model but clearly demonstrate non-chiral current contributions away from the plateaus of quantized Hall resistance. This work contributes to a deeper understanding of the microscopic dynamics and the distribution of current density inside realistic mesoscopic devices in the regime of the QHE.

ACKNOWLEDGEMENT

The authors thank Piet Brouwer for help with the coherent model and Afif Siddiki for fruitful discussions. This work was funded by the Deutsche Forschungsgemeinschaft (DFG, German Research Foundation) – 218453298.

CONTRIBUTIONS OF THE AUTHORS

V. Y. U. supplied the wafer. S. S. and M. K. performed the measurements. S. S. and S. L. analyzed the data. S. L. derived the models. S. S. and S. L. wrote the article.

REFERENCES

-
- [1] M. Büttiker, Four-terminal phase-coherent conductance, *Phys. Rev. Lett.* **57**, 1761 (1986).
- [2] M. Büttiker, Absence of backscattering in the quantum Hall effect in multiprobe conductors, *Phys. Rev. B* **38**, 9375 (1988).
- [3] D. B. Chklovskii, B. I. Shklovskii, and L. I. Glazman, Electrostatics of edge channels, *Phys. Rev. B* **46**, 4026 (1992).
- [4] D. B. Chklovskii, K. A. Matveev, and B. I. Shklovskii, Ballistic conductance of interacting electrons in the quantum Hall regime, *Phys. Rev. B* **47**, 12605 (1993).
- [5] M. M. Fogler and B. I. Shklovskii, Resistance of a long wire in the quantum Hall regime, *Phys. Rev. B* **50**, 1656 (1994).
- [6] K. Lier and R. R. Gerhardts, Self-consistent calculations of edge channels in laterally confined two-dimensional electron systems, *Phys. Rev. B* **50**, 7757 (1994).
- [7] A. Siddiki and R. R. Gerhardts, Thomas-fermi-poisson theory of screening for laterally confined and unconfined two-dimensional electron systems in strong magnetic fields, *Phys. Rev. B* **68**, 125315 (2003).
- [8] A. Siddiki and R. R. Gerhardts, Incompressible strips in dissipative Hall bars as origin of quantized Hall plateaus, *Phys. Rev. B* **70**, 195335 (2004).
- [9] R. R. Gerhardts, The effect of screening on current distribution and conductance quantisation in narrow quantum Hall systems, *physica status solidi (b)* **245**, 378 (2008), <https://onlinelibrary.wiley.com/doi/pdf/10.1002/pssb.200743344>.
- [10] P. Weitz, E. Ahlswede, J. Weis, K. Klitzing, and K. Eberl, Hall-potential investigations under quantum Hall conditions using scanning force microscopy, *Physica E: Low-dimensional Systems and Nanostructures* **6**, 247 (2000).
- [11] E. Ahlswede, P. Weitz, J. Weis, K. von Klitzing, and K. Eberl, Hall potential profiles in the quantum Hall regime measured by a scanning force microscope, *Physica B: Condensed Matter* **298**, 562 (2001), international Conference on High Magnetic Fields in Semiconductors.
- [12] E. Ahlswede, J. Weis, K. v. Klitzing, and K. Eberl, Hall potential distribution in the quantum Hall regime in the vicinity of a potential probe contact, *Physica E: Low-dimensional Systems and Nanostructures* **12**, 165–168 (2002), proceedings of the Fourteenth International Conference on the Electronic Properties of Two-Dimensional Systems.
- [13] S. Sirt, V. Y. Umansky, A. Siddiki, and S. Ludwig, Direct measurement of bulk currents in the quantized hall regime (2024), [arXiv:2405.05138](https://arxiv.org/abs/2405.05138).
- [14] Y. Ji, Y. Chung, D. Sprinzak, M. Heiblum, D. Mahalu, and H. Shtrikman, An electronic Mach-Zehnder interferometer, *Nature* **422**, 415–418 (2003).
- [15] The slight deviations between the two are likely related with local changes in the sample during thermal cycles of the He-3 evaporation cryostat to $T > 4$ K between the two measurements.
- [16] K. von Klitzing, Developments in the quantum hall effect, *Philosophical Transactions of the Royal Society A: Mathematical, Physical and Engineering Sciences* **363**, 2203 (2005), <https://royalsocietypublishing.org/doi/pdf/10.1098/rsta.2005.1640>.
- [17] K. L. McCormick, M. T. Woodside, M. Huang, M. Wu, P. L. McEuen, C. Duruo, and J. S. Harris, Scanned potential microscopy of edge and bulk currents in the quantum Hall regime, *Phys. Rev. B* **59**, 4654 (1999).
- [18] J. Horas, A. Siddiki, J. Moser, W. Wegscheider, and S. Ludwig, Investigations on unconventional aspects in the quantum hall regime of narrow gate defined channels, *Physica E: Low-dimensional Systems and Nanostructures* **40**, 1130 (2008), 17th International Conference on Electronic Properties of Two-Dimensional Systems.
- [19] A. Siddiki, J. Horas, J. Moser, W. Wegscheider, and S. Ludwig, Interaction-mediated asymmetries of the quantized hall effect, *EPL (Europhysics Letters)* **88**, 17007 (2009).
- [20] A. Siddiki, J. Horas, D. Kupidura, W. Wegscheider, and S. Ludwig, Asymmetric nonlinear response of the quantized hall effect, *New Journal of Physics* **12**, 113011 (2010).
- [21] J. Weis and K. von Klitzing, Metrology and microscopic picture of the integer quantum Hall effect, *Philosophical Transactions of the Royal Society A: Mathematical, Physical and Engineering Sciences* **369**, 3954 (2011), <https://royalsocietypublishing.org/doi/pdf/10.1098/rsta.2011.0198>.
- [22] Kendirlik E. M., Sirt S., Kalkan S. B., Dietsche W., Wegscheider W., Ludwig S., and Siddiki A., Anomalous resistance overshoot in the integer quantum Hall effect, *Scientific Reports* **3**, 3133 (2013).
- [23] E. M. Kendirlik, S. Sirt, S. B. Kalkan, N. Ofek, V. Umansky, and A. Siddiki, The local nature of incompressibility of quantum Hall effect, *Nature Communications* **8**, 14082 (2017).